Journal of Molecular Graphics and Modelling 35 (2012) 43–48

Contents lists available at SciVerse ScienceDirect

Journal of Molecular Graphics and Modelling

journal homepage: www.elsevier.com/locate/JMGM

The adenosine deaminases of *Plasmodium vivax* and *Plasmodium falciparum* exhibit surprising differences in ligand specificity

Andrei Ivanov [1], Ichiro Matsumura *

Emory University School of Medicine, Department of Biochemistry, Center for Fundamental and Applied Molecular Evolution, 1510 Clifton Road NE, Atlanta, GA 30322, USA

ARTICLE INFO

Article history:
Received 30 September 2011
Received in revised form 13 February 2012
Accepted 16 February 2012
Available online 28 February 2012

Keywords:
Computational modeling
Drug design
Ligand recognition
Selective inhibition
Site-directed mutagenesis
Adenosine deaminase

ABSTRACT

Plasmodium vivax and *Plasmodium falciparum* cause malaria, so proteins essential for their survival *in vivo* are potential anti-malarial drug targets. Adenosine deaminases (ADA) catalyze the irreversible conversion of adenosine into inosine, and play a critical role in the purine salvage pathways of Plasmodia and their mammalian hosts. Currently, the number of selective inhibitors of Plasmodium ADAs is limited. One potent and widely used inhibitor of the human ADA (hADA), erythro-9-(2-hydroxy-3-nonly)adenine (EHNA), is a very weak inhibitor (K_i = 120 μM) of *P. falciparum* ADA (pfADA). EHNA-like compounds are thus excluded from consideration as potential inhibitors of Plasmodium ADA in general. However, EHNA activity in *P. vivax* ADA (pvADA) has not been reported. Here we applied computational molecular modeling to identify ligand recognition mechanisms unique to *P. vivax* and *P. falciparum* ADA. Our biochemical experiments show that EHNA is at least 60-fold more potent against pvADA (K_i = 1.9 μM) than against pfADA. The D172A pvADA mutant is bound even more tightly (K_i = 0.9 μM). These results improve our understanding of the mechanisms of ADA ligand recognition and species-selectivity, and facilitate the rational design of novel EHNA-based ADA inhibitors as anti-malarial drugs. To demonstrate a practical application of our findings we have computationally predicted a novel potential inhibitor of pvADA that will not interact with the human ADA.

1. Introduction

The World Health Organization (WHO) reported 243 million cases of malaria around the world in 2008. Approximately one million were fatal. Four distinct Plasmodium species cause human malaria: *Plasmodium falciparum*, *Plasmodium vivax*, *Plasmodium malariae*, and *Plasmodium ovale*. Among them, *P. vivax* and *P. falciparum* are the most common. *P. vivax* is more widely distributed, but *P. falciparum* is the deadliest [1,2]. Recently, Das et al. highlighted interesting differences in the whole genome sequences of *P. vivax* and *P. falciparum* [3]. *P. vivax* contains 23% less A + T nucleotide content than *P. falciparum*; 82% *P. vivax* and *P. falciparum* genes are conserved, while 18% genes are species specific. These genomic dissimilarities suggest that proteins of these two parasites can differ significantly in structure, and thus, in their molecular mechanisms of ligand recognition.

All four Plasmodium species express adenosine deaminase (ADA), which catalyzes the deamination of adenosine (**1**, Scheme 1) to form inosine. This reaction is part of the essential purine salvage pathway. ADA inhibition is fatal to the parasite, so ADA is a promising target for malaria treatment [4,5]. The rational design of Plasmodium-specific ADA inhibitors, however, remains a challenge. In contrast, many potent hADA inhibitors have been proposed [6,7]. Deoxycoformycin, a transition-state analogue (also known as pentostatin, **2**), is among the best-known and most potent inhibitors of hADA and pADA. The structure of its complex with the pvADA was recently solved [8,9]. Erythro-9-(2-hydroxy-3-nonly)adenine (EHNA, **3**) is another well known and widely used inhibitor of hADA. It is, however, almost inactive against pfADA [5,10]. Most assume that it lacks activity against the other Plasmodium ADAs, but this assumption has not to our knowledge been tested experimentally. Here we describe computational and biological studies of ligand recognition by pvADA and pfADA.

2. Experimental procedures

2.1. Sequence alignment and homology modeling

The sequences of pvADA and pfADA (UNIPROT ID: A5KE01 and Q8IJA9, respectively) were aligned with ClustalX, using the BLOSUM Protein Weight Matrix (Scheme 2) [11]. Modeller 9.7 [12] (number of models to generate = 25, library_schedule = autosched.slow, max_var_interactions = 10,000,

* Corresponding author. Tel.: +1 404 727 5625; fax: +1 404 727 3452.
E-mail address: imatsum@emory.edu (I. Matsumura).
[1] Present address: Emory Chemical Biology Discovery Center, Emory University School of Medicine, 1462 Clifton Road NE, Atlanta, Georgia 30322, USA.

1093-3263/$ – see front matter © 2012 Elsevier Inc. All rights reserved.
doi:10.1016/j.jmgm.2012.02.004

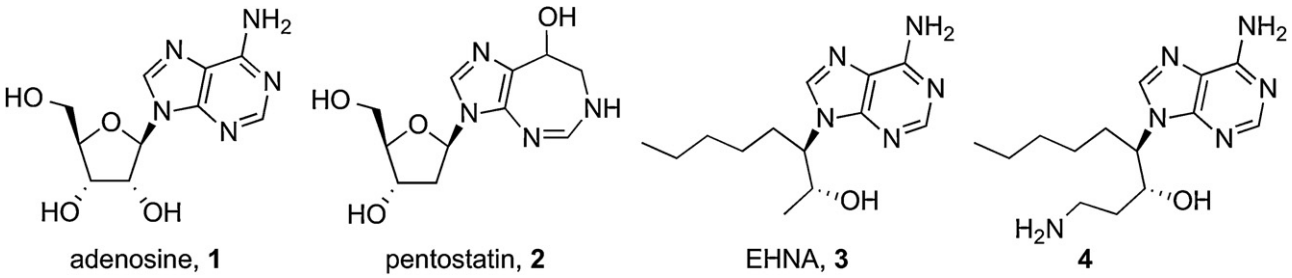

Scheme 1. The ligands of adenosine deaminase: a native substrate, adenosine (**1**), transition-state analogue inhibitor, pentostatin (**2**), a potent inhibitor of hADA, EHNA (**3**), a novel potential inhibitor of pvADA (**4**).

md_level = refine. very_slow) was used to construct a homology model of pfADA based on the crystal structure of pvADA (PDB ID: 2PGR) [9]. Water molecule #687, which appeared in the pvADA-adenosine and pvADA-pentostatin crystal structures [9], zinc cation, and the pentostatin ligand were included in our model. The most accurate model was selected based on the DOPE, GA341, and normalized DOPE scoring function values calculated for each model. The geometries of the amino acid residues were also evaluated with the Ramachandran plot generated with the Maestro program of the Schrödinger Suite [13]. The pvADA crystal structure and pfADA model were further refined with the Protein Preparation Wizard (Schrödinger Suite) [14].

Inhibitors were docked to protein structures using the Glide program of the Schrödinger Suite [15]. The pfADA model was superimposed upon the crystal structure of pvADA bound to adenosine (compound **1** in Scheme 1). Thus, **1** was prepositioned inside the pfADA binding site. For both proteins, the protein grid generation was performed for the box with the center in the centroid of **1**. The box size was determined automatically. The value of 1.0 and 0.8 were used for receptor and ligand van der Waals scaling, respectively. The extra precision (XP) mode of Glide was used with its default values for all parameters. All ligands were prepared using LigPrep program of the Schrödinger Suite [16]. The protein–ligand complexes obtained after molecular docking were optimized with the Powell–Reeves conjugate gradient energy minimization method using the maximum of 2000 interactions and the value of threshold of 0.05. The same procedure was utilized for molecular docking of compound **4** to pvADA and hADA (PDB ID: 3IAR) crystal structures.

2.2. Protein cloning and site-directed mutagenesis

The 1116 bp pvADA cDNA was synthesized (GeneArt, Regensburg, Germany), and inserted into the pET28a(+) expression vector (Novagen, Madison, WI) between its NdeI and XhoI sites. The pvADA D172A mutant was constructed by QuikChange site-directed mutagenesis [17]. The PCR reaction was performed with the Phusion DNA polymerase, and a pair of primers (mutated codons are underlined):

5′-cctgatgtgcattggtgctaccggtcatgaagcag-3′ and
5′-ctgcttcatgaccggtagcaccaatgcacatcagg-3′.

The custom synthesis of oligonucleotides was ordered from the Integrated DNA Technologies Inc. (Coralville, IA, USA). The mutation was confirmed by sequence analysis (Macrogen, Rockville, MD, USA).

2.3. Protein expression and purification

Escherichia coli BL21(DE3) Gold cells (Strategene, La Jolla, CA) were transformed with pvADA-pET28a(+) plasmids encoding the wild-type and D172A mutant proteins. The transformed cells were propagated to mid-log phase (OD_{600} = 0.6) at 37 °C in 200 mL LB medium supplemented with 50 μg/mL kanamycin, and 1 mM zinc sulfate. Gene expression was induced for 20 h with 1 mM isopropyl-1-thio-b-D-galactopyranoside (IPTG). The cells were harvested by centrifugation, resuspended in 20 mL of the Ni^{+2}-binding buffer [10 mM imidazole, 50 mM potassium phosphate, 300 mM sodium

```
pvADA 1   -----MNILQEPIDFLKKEELKNIDLSQMSKKERYKIWKRIPKCELHCHLDLCFSADFFVSCIRKYNLQP  65
pfADA 1   MNCKNMDTSYEIINYLTKDELD-IDLSCMDKKERYKIWKRLPKCELHCHLDVCFSVDFFLNVIRKYNIQP  69
               *    * *  * * **  **** * ********** ********** *** ***   ***** **

pvADA 66  NLSDEEVLDYYLFAKGGKSLGEFVEKAIKVADIFHDYEVIEDLAKHAVFNKYKEGVVLMEFRYSPTFVAF 135
pfADA 70  NMSDEEIIDYYLFSKPGKSLDEFVEKALRLTDIYIDYTVVEDLAKHAVFNKYKEGVVLMEFRYSPSFMSF 139
          * ****  ***** * **** ******    **  ** * ************************ *  *

pvADA 136 KYNLDIELIHQAIVKGIKEVVELLDHKIHVALMCIGDTGHEAANIKASADFCLKHKADFVGFDHGGHEVD 205
pfADA 140 KHNLDKDLIHEAIVKGLNEAVALLEYKIQVGLLCTGDGGLSHERMKEAAEFCIKHKKDFVGYDHAGHEVD 209
          * ***  *** *****  * * **  ** * * * ** *      *  * ** *** **** ** *****

pvADA 206 LKEYKEIFDYVRESGVPLSVHAGEDVTLPNLNTLYSAIQVLKVERIGHGIRVAESQELIDMVKEKNILLE 275
pfADA 209 LKPFKDIFDNIREEGISLSVHAGEDVSIPNLNSLYTAINLLHVKRIGHGIRVSESQELIDLVKEKDILLE 279
          **  * ***  ** *  *********  **** ** **  * * ******** ******* **** ****
```

Scheme 2. The amino acid sequence alignment of pvADA and pfADA was used to construct the homology model of pfADA. The overall sequence identity is 72%. The residues located in the binding site and which are not identical in these to proteins are shown in bold.

chloride, pH 7.5], and lysed in two passages through a French Press pressure cell. The cell debris was removed by centrifugation (14,000 g, 1 h).

The supernatant was filtered through a 20 μm filter, and passed twice through the 5 mL HiTrap Ni-NTA column (GE Healthcare, Uppsala, Sweden). To exclude cross-contamination during purification two different HiTrap Ni-NTA columns were used for pvADA wild-type and D172A mutant. The column-bound protein was washed with 60 mL of buffer [20 mM imidazole, 50 mM potassium phosphate, 300 mM sodium chloride, pH 7.5]. The proteins were eluted with 15 mL of elution buffer [500 mM imidazole, 50 mM potassium phosphate, 300 mM sodium chloride, pH 7.5]. The pvADA WT and D172A mutant were concentrated with 30 K concentration units (Milipore, Billerica, MA, USA) to final volumes of 500 μL and subjected to the size-exclusion chromatography with the ÄKTA purifier using Superdex 200 16/60 column (GE Healthcare) and an appropriate buffer [50 mM potassium phosphate pH 7.5, 300 mM sodium chloride]. The 800 μL fractions were collected and analyzed with the silver-stained SDS-PAGE gel electrophoresis. The purest fractions were combined and concentrated with the 30 K Millipore concentration units. The final concentrations of his-tagged wild-type pvADA (2.8 mg/mL) and D172A mutant (3.2 mg/mL) were measured with the Bradford method using BSA as a standard.

2.4. Enzymatic assay

Adenosine and EHNA were purchased from Sigma–Aldrich (St. Louis, MO, USA) and Santa-Cruz Biotechnology Inc. (Santa Cruz, CA, USA), respectively. Enzymatic activities were analyzed with a Shimadzu UV-1601 spectrophotometer by measuring the rate of ADA-dependent decrease of adenosine (absorbance at 265 nm at 30 °C in quartz cuvettes with a path length of 1 cm). Assays were performed in 50 mM potassium phosphate buffer pH 7.5. To calculate the K_M value, pvADA WT activities were measured over six different concentrations of adenosine (from 0.5 to 2.5 × K_M). Six concentrations of EHNA (from 0 to 50 μM), and 100 μM adenosine were used to calculate the binding constants of EHNA at pvADA WT and D172A mutant. In all measurements 11.8 nM (0.5 μg/mL) enzyme was used. Assays were repeated at least three times.

3. Results and discussion

3.1. Molecular modeling of pvADA and pfADA

EHNA is a very weak inhibitor of pfADA, but its reactivity with pvADA has not been reported. The crystal structure of pvADA was recently solved, but that of pfADA has not. It seemed likely that the two enzymes were quite similar in the configuration of their ligand binding sites, so we constructed a homology model of pfADA based upon the crystal structure of pvADA. The amino acid sequences of pvADA and pfADA share 72% identity, but superimposition of the three-dimensional structures of these two enzymes revealed that several amino acid residues in the binding pockets differ. In particular, Val51, Leu97, Thr174, Ile179, Ala204 of pfADA were found in positions occupied by Leu47, Ile93, Ile170, His175, Gly200 of pvADA, respectively (Scheme 2, Fig. 1). All of these residues are located within 3 Å from the atoms of **1** in the pvADA crystal structure, and are thus directly involved in ligand recognition.

Computational molecular docking was utilized to investigate the inhibitor binding modes of pvADA and pfADA. Initially, to confirm the reliability of the docking procedure, **2** was extracted from and re-docked to the crystal structure of pvADA. As expected, the re-docked structure was identical to its experimentally determined position in the pvADA crystal structure (RMSD = 0.2 Å). Then, **2** was

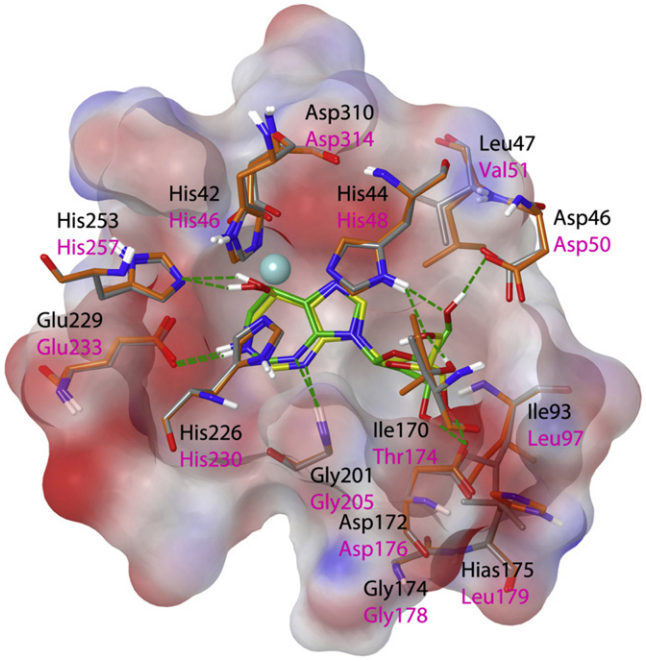

Fig. 1. The superimposition of the ligand binding sites of the crystal structure of pvADA complexed with pentostatin (protein atoms are colored in orange, pentostatin carbon atoms – in green) and a homology model of pfADA with the docked pentostatin (protein atoms are colored in grey, pentostatin carbon atoms – in yellow). The amino acid residues of pvADA and pfADA are labeled in black and magenta, respectively. The H-bonds are indicated by green lines.

docked to the binding pocket of pfADA. The binding mode of **2** with pfADA obtained after molecular docking was very similar to the one observed in pvADA crystal structure ($RMSD_{HEAVY-ATOM}$ = 0.7 Å). The 3′—OH group of **2** formed a hydrogen bond with the carboxylic group of Asp172. The OH-group at position six was H-bonded to His257, and an amino group at the 1-position of pentostatin formed a hydrogen bond with Glu233. Also, the N3 nitrogen atom was hydrogen bonded to the NH-group of Gly205 of pfADA.

The binding modes of **2** with pvADA and pfADA differed most in the coordination of the 5′—OH group – the corresponding oxygen atoms differed in position by 1.65 Å. In the pvADA crystal structure the hydroxyl group of **2** formed H-bonds with the carboxylic group of Asp46 and the imidazole ring of His44, and was located more than 3 Å from the hydrophobic Ile170. In contrast, the pfADA structure showed Thr174 in the position of pvADA Ile170. The 5′—OH group of **2** was located between the imidazole ring of His48 and the OH-group of Thr174, forming hydrogen bonds with both residues. It did not, however, form a H-bond with Asp46 of pfADA. The structural differences between the pvADA and pfADA complexes with pentostatin correspond to a 2-fold difference in the energy scoring function calculated for the **2**/pfADA (Glide_emodel = −64) and 2/pvADA (Glide_emodel = −106) complexes. This calculation is also in agreement with the binding constants reported for coformycin in pfADA (K_I = 14 nM) and pvADA (K_I = 7.4 nM) [8]. These findings indicate that modest differences in binding site composition can produce observable effects on ligand binding modes, even for a transition-state analogue inhibitor such as **2**.

The molecular docking results of **2** with pvADA and pfADA were in good agreement with the crystal structure of pvADA-**2** complex, so we used the same procedure to study the binding mode of **3** with these proteins. Although **3** is a very weak inhibitor of pfADA, it still can bind to the ligand-binding pocket with the K_I value of 120 μM [10]. In both the pfADA and pvADA complexes, the adenine ring of **3** occupied the same position as the corresponding ring of **2** (Fig. 2). In contrast, the nonan-2-ol fragment of **3** was

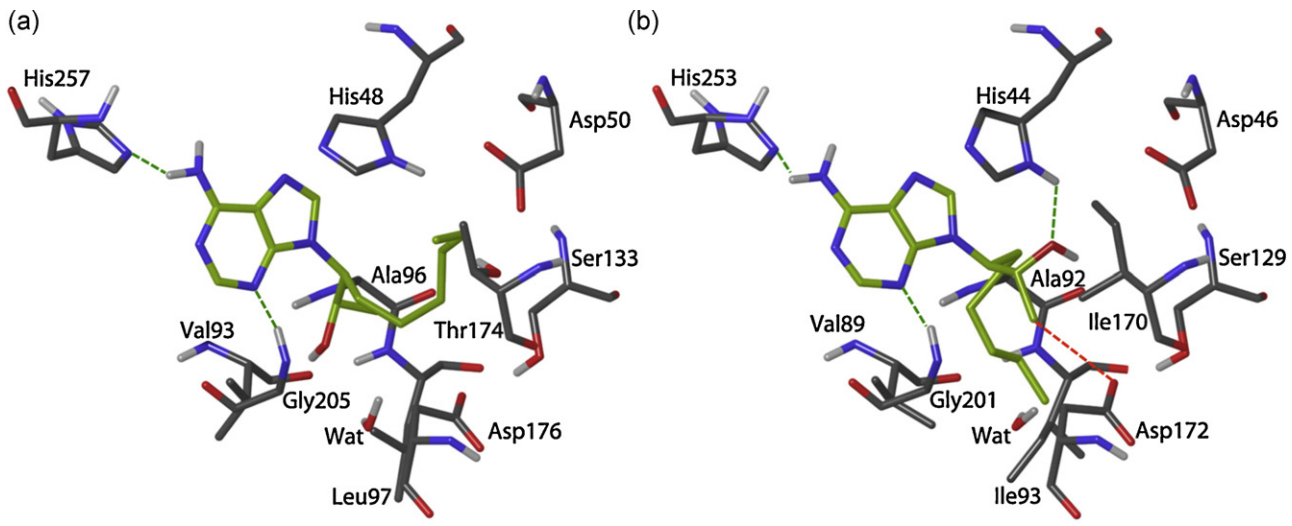

Fig. 2. The putative binding mode of EHNA (**2**) with the molecular model of pfADA (a) and the crystal structure of pvADA (b). In the model of pfADA, the hydrophobic chain of **2** was unfavorably oriented toward hydrophilic residues, and the ligand hydroxyl group was observed in proximity to hydrophobic Val93 and Ala96. In contrast, this hydroxyl group of **2** formed a hydrogen bond with His44 of pvADA (H-bonds are indicated by green lines), and the hydrophobic chain of the ligand was located near hydrophobic amino acid residues. The methyl group of **2** was located at a distance of 3.2 Å from the carboxylic oxygen atoms of Asp172 (indicated by a red line).

oriented differently in those two models. In the pfADA-**2** complex, the hydrophobic heptyl chain of the nonan-2-ol fragment was found in an unfavorable position between hydrophilic functional groups of His48, Asp50, Ser133, Thr174, and Asp176. The hydroxyl group of the nonan-2-ol moiety was oriented toward the water molecule, and the hydrophobic side chains of Val93 and Ala96. Furthermore, the position of this ligand OH-group did not correspond to any of the functional groups of **2**.

The nonan-2-ol fragment assumed the opposite orientation in the pvADA-**3** model. In particular, the long hydrophobic heptyl chain of the nonan-2-ol fragment appeared in proximity to hydrophobic amino acid residues, namely Phe88, Val89, Ala92, Ile93, and Phe132. The significant difference in the orientations of the nonan-2-ol fragment of **3** in two similar binding sites should not be surprising. The crystal structures of pvADA bound to **2** or its methylthio-analogue (MT-coformycin) indicated that the ribose fragment, which is analogous to the nonan-2-ol fragment of **3**, assumed a completely different orientation in the same binding pocket [8]. The methyl group of the nonan-2-ol chain of **2** was found in unfavorable proximity (3.2 Å) to the carboxylic oxygen atom of Asp172. In contrast, the hydroxyl group of the nonan-2-ol fragment was located near His44, and formed a hydrogen bond with its imidazole ring. The same hydrogen bond was observed for the 5′—OH group of **2** in the crystal structure of pvADA. The superimposition of **2** and **3** inside the binding center of pvADA demonstrated that the OH-group of the nonan-2-ol moiety of **3** was located between the oxygen atoms of 5′—OH group and the ribose ring of **2**.

These observations also agree with the values of the energy scoring functions obtained for the models. The Glide XP scoring function calculated for **2** and **3** docked to pvADA differed by 18%; in pfADA models the difference of 31% was observed (the values of the Glide XP scoring function calculated for **2** were defined to be 100%). Thus, our qualitative and quantitative molecular docking analysis revealed differences in the binding mode of **3** with pvADA and pfADA. It also suggested that configuration of pvADA binding site is more favorable for **3** than the ligand binding center of pfADA, and that more potent inhibition of pvADA by **3** can be expected.

3.2. Kinetic assay

Recently, the important role of Asp172 pvADA ligand recognition was reported by Larson et al. [9]. Our molecular modeling analysis suggested that the carboxylic oxygen atom of Asp172 unfavorably interacted with the hydrophobic methyl group of **3**. To further understand the functional role of Asp172 in the ADA structure we performed site-directed mutagenesis, heterologous expression and *in vitro* kinetic characterization. The wild-type and D172A mutant forms of pvADA were expressed in BL21(DE3) Gold cells (as described in the Section 2.3), and purified by Ni^{2+}-affinity chromatography and the size-exclusion chromatography on a Superdex 200 column. The purity of the protein was confirmed by SDS-PAGE gel electrophoresis (Fig. 3). The K_M and k_{cat} values of the wild-type and D172A pvADA variants in reactions with EHNA have been previously reported. For this reason, we did not perform precise steady-state kinetics experiments here.

We measured the K_M value of WT pvADA in reactions with adenosine to confirm that our techniques were consistent with that of published work. Our value ($K_M = 71 \pm 16$ μM) was congruent with that reported by Ho et al. ($K_M = 60 \pm 6$ μM) [8]. We also compared the adenosine deamination activities of the WT and D172A pvADA enzymes by monitoring the changes in absorbance at 260 nm during the reaction of 100 μM adenosine with 11.8 nM enzyme. In agreement with the published data [8], the D172A pvADA mutant was 40% less active than the wild type. Thus, these experiments confirmed the consistency of our data with the previously reported results, and encouraged us to use both proteins in further enzyme inhibition assays.

We observed an inhibitory effect of **3** in a concentration range from 0.1 to 50 μM on the ADA deamination activity in the reactions of pvADA WT and D172A mutant with 100 μM adenosine. In contrast to the previous data reported for *P. falciparum* ADA, significant inhibition (more than 20%) was observed for pvADA WT with low (0.5 μM) concentrations of **3**. Moreover, only 10% of the enzyme activity remained in the presence of 50 μM **3**. The inhibition of the pvADA D172A mutant was even more potent. In particular, the addition of **3** at 0.5uM concentration decreased the mutant activity by 31%, and at 50 μM concentration pvADA activity was not detectable. The calculated K_I values (Fig. 3) show that pvADA WT ($K_I = 1.9$ μM) and pvADA D172A mutant ($K_I = 0.9$ μM) are more susceptible to inhibition by **3** than pfADA WT ($K_I = 120$ μM). Interestingly, Asp172 is conserved among all plasmodium ADAs, but the human ADA has Met at that position. The D172A mutation in pvADA abrogates binding to methylthiocoformycin or methylthioadenosine [8].

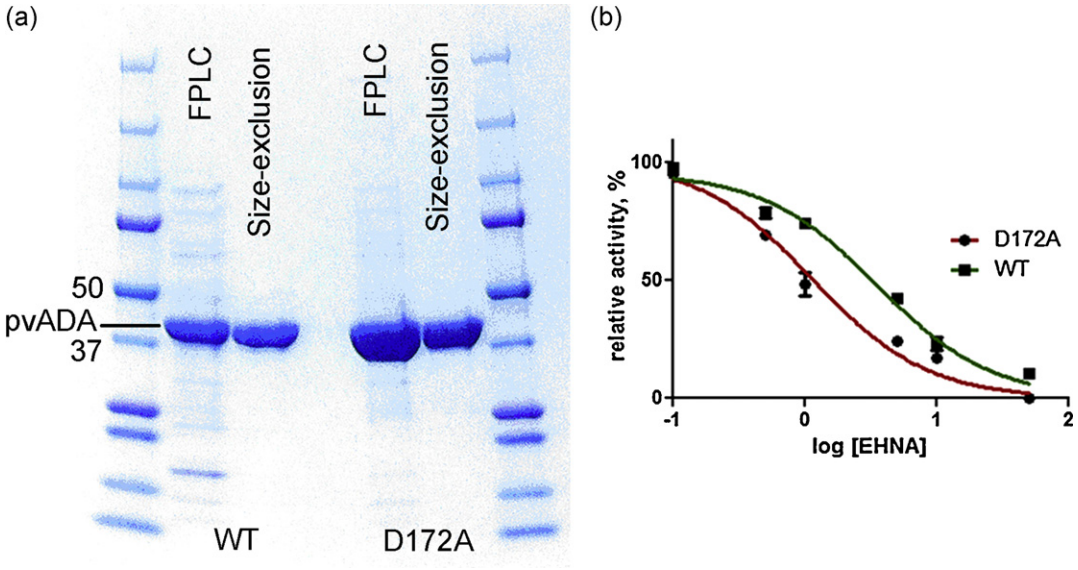

Fig. 3. The purity of pvADA WT and D172 mutant obtained after immobilized metal affinity chromatography and gel filtration was confirmed by SDS-PAGE (a). Inhibitory curves (b) were obtained for the pvADA WT and D172A mutant in reactions with 100 μM adenosine and EHNA at concentrations of 0.1–50 μM. Assays were performed in 50 mM potassium phosphate buffer pH 7.5. Six concentrations of EHNA (from 0 to 50 μM), and 100 μM adenosine were used to measure the binding constants of EHNA at pvADA WT and D172A mutant. In all measurements 11.8 nM enzyme (0.5 μg per cuvette) was used. All assays were repeated at least three times.

3.3. Computational design of novel selective inhibitor of pvADA

We designed a putative selective inhibitor of pvADA inhibitor to illustrate the practical applications of our findings. We modified **3** by substituting the methyl group of the nonan-2-ol chain with an ethylamine fragment. The resulting compound **4** (Scheme 1) was docked to the pvADA and hADA crystal structures. Molecular docking showed that **4** fits the pvADA binding site with the same binding mode as **3** (Fig. 4). In addition, the newly introduced amino group of **4** formed new H-bonds with the Asp172 and Ser129 side chains. In contrast, this compound was unable to fit the binding site of hADA (no reasonable binding mode was detected with the molecular docking). We predict that **4** will bind pvADA with greater affinity than EHNA, **3**, and exhibit much less reactivity against hADA. We intend to validate this prediction in future studies.

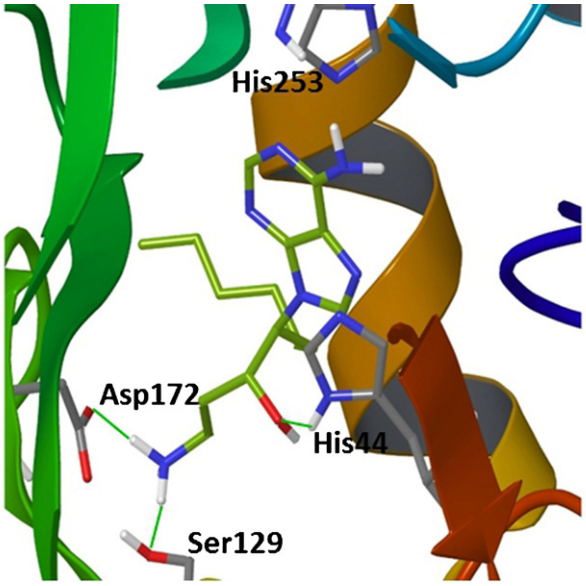

Fig. 4. A hypothetical inhibitor of pvADA, **4**, proposed here, was computationally docked into pvADA crystal structure. The general binding mode of **4** is identical to the binding mode of its parent compound **3**. In addition new H-bonds were formed between the amino group of **4** and Asp172 and Ser129 side chains.

In summary, our studies have indicated significant differences in structural organization and molecular mechanisms of ligand recognition of plasmodium adenosine deaminases. We observed a 60-fold difference in EHNA binding affinity of pvADA and pfADA. We expect that other EHNA-based compounds, such as **4**, could provide higher affinity and selectivity for Plasmodium ADA versus its human ortholog. Previous workers showed that Asp172 enables binding interactions with adenosine derivatives, including a transition-state analogue pentostatin [9]. Our data reveals the critical role of Asp172 in recognition of inhibitors, which are structurally distinct from adenosine due to the absence of the ribose ring. We therefore speculate this residue would similarly play a decisive role in a selective binding of any substrate or inhibitor to adenosine deaminase of plasmodium parasites. The divergent amino acid residues located in this position in the plasmodium (Asp) and human (Met) homologues provide an opportunity for rational design of novel anti-malarial drugs.

Acknowledgments

We are thankful to Dr. Vern Schramm (Department of Biochemistry, Albert Einstein College of Medicine, Bronx, NY) and Dr. Maria Belen Cassera (Department of Biochemistry, Fralin Biotechnology Center, Virginia Polytechnic Institute and State University, Blacksburg, VA) for invaluable suggestions and guidance on the biological studies of adenosine deaminase. We are also thankful to Dr. Kenneth A. Jacobson and Dr. Stefano Costanzi (Natinal Institute of Diabetes, Digestive and Kidney Diseases, National Institutes of Health, Bethesda, MD) for reading the manuscript. AI and IM were supported by a grant from the NIGMS (1 R01 GM086824).

References

[1] N. Singh, A.P. Dash, K. Thimasarn, Fighting malaria in Madhya Pradesh (Central India): are we losing the battle? Malar. J. 8 (2009) 93.

[2] S. Tesfaye, Y. Belyhun, T. Teklu, T. Mengesha, B. Petros, Malaria prevalence pattern observed in the highland fringe of Butajira, Southern Ethiopia: a longitudinal study from parasitological and entomological survey, Malar. J. 10 (2011) 153.

[3] A. Das, M. Sharma, B. Gupta, A.P. Dash, *Plasmodium falciparum* and *Plasmodium vivax*: so similar, yet very different, Parasitol. Res. 105 (2009) 1169–1171.

[4] D.C. Madrid, L.M. Ting, K.L. Waller, V.L. Schramm, K. Kim, *Plasmodium falciparum* purine nucleoside phosphorylase is critical for viability of malaria parasites, J. Biol. Chem. 283 (2008) 35899–35907.

[5] L.M. Ting, W. Shi, A. Lewandowicz, V. Singh, A. Mwakingwe, M.R. Birck, E.A. Ringia, G. Bench, D.C. Madrid, P.C. Tyler, G.B. Evans, R.H. Furneaux, V.L. Schramm, K. Kim, Targeting a novel *Plasmodium falciparum* purine recycling pathway with specific immucillins, J. Biol. Chem. 280 (2005) 9547–9554.

[6] S. Costanzi, C. Lambertucci, R. Volpini, S. Vittori, G. Lupidi, G. Cristalli, 3'-deoxyribofuranose derivatives of 1-deaza and 3-deaza-adenosine and their activity as adenosine deaminase inhibitors, Nucleosides Nucleotides Nucleic Acids 20 (2001) 1037–1041.

[7] G. Cristalli, S. Costanzi, C. Lambertucci, G. Lupidi, S. Vittori, R. Volpini, E. Camaioni, Adenosine deaminase: functional implications and different classes of inhibitors, Med. Res. Rev. 21 (2001) 105–128.

[8] M.C. Ho, M.B. Cassera, D.C. Madrid, L.M. Ting, P.C. Tyler, K. Kim, S.C. Almo, V.L. Schramm, Structural and metabolic specificity of methylthiocoformycin for malarial adenosine deaminases, Biochemistry 48 (2009) 9618–9626.

[9] E.T. Larson, W. Deng, B.E. Krumm, A. Napuli, N. Mueller, W.C. Van Voorhis, F.S. Buckner, E. Fan, A. Lauricella, G. DeTitta, J. Luft, F. Zucker, W.G. Hol, C.L. Verlinde, E.A. Merritt, Structures of substrate- and inhibitor-bound adenosine deaminase from a human malaria parasite show a dramatic conformational change and shed light on drug selectivity, J. Mol. Biol. 381 (2008) 975–988.

[10] P.E. Daddona, W.P. Wiesmann, C. Lambros, W.N. Kelley, H.K. Webster, Human malaria parasite adenosine deaminase. Characterization in host enzyme-deficient erythrocyte culture, J. Biol. Chem. 259 (1984) 1472–1475.

[11] M.A. Larkin, G. Blackshields, N.P. Brown, R. Chenna, P.A. McGettigan, H. McWilliam, F. Valentin, I.M. Wallace, A. Wilm, R. Lopez, J.D. Thompson, T.J. Gibson, D.G. Higgins, W. Clustal, X. Clustal, version 2.0. Bioinformatics 23 (2007) 2947–2948.

[12] A. Sali, T.L. Blundell, Comparative protein modelling by satisfaction of spatial restraints, J. Mol. Biol. 234 (1993) 779–815.

[13] Maestro, version 9.2, Schrödinger, LLC, New York, NY, 2011.

[14] Schrödinger Suite 2009 Protein Preparation Wizard; Epik version 2.0, S., LLC, New York, NY, 2009; Impact version 5.5, Schrödinger, LLC, New York, NY, 2009; Prime version 2.1, Schrödinger, LLC, New York, NY, 2009.

[15] R.A. Friesner, J.L. Banks, R.B. Murphy, T.A. Halgren, J.J. Klicic, D.T. Mainz, M.P. Repasky, E.H. Knoll, M. Shelley, J.K. Perry, D.E. Shaw, P. Francis, P.S. Shenkin, Glide: a new approach for rapid, accurate docking and scoring. 1. Method and assessment of docking accuracy, J. Med. Chem. 47 (2004) 1739–1749.

[16] LigPrep, version 2.4, Schrödinger, LLC, New York, NY, 2010.

[17] D. Papworth, J.C. Bauer, J. Braman, D.A. Wright, Site-directed mutagenesis in one day with greater than 80% efficiency, Strategies 9 (1996) 3–4.